Atmos. Chem. Phys. Discuss., 13, 31527–31562, 2013
www.atmos-chem-phys-discuss.net/13/31527/2013/
doi:10.5194/acpd-13-31527-2013

Atmospheric Chemistry and Physics Discussions

Role of the residual layer and large-scale subsidence on the development and evolution of the convective boundary layer

E. Blay-Carreras[1], D. Pino[1,2], A. Van de Boer[3], O. De Coster[3], C. Darbieu[4], O. Hartogensis[3], F. Lohou[4], M. Lothon[4], H. Pietersen[3], and J. Vilà-Guerau de Arellano[3]

[1]Department of Applied Physics, Universitat Politècnica de Catalunya·BarcelonaTech, Barcelona, Spain
[2]Institute of Space Studies of Catalonia (IEEC-UPC), Barcelona, Spain
[3]Meteorology and Air Quality Group, Wageningen University, Wageningen, the Netherlands
[4]Laboratoire d'Aérologie, Université de Toulouse and CNRS, Toulouse, France

Received: 5 November 2013 – Accepted: 18 November 2013 – Published: 2 December 2013

Correspondence to: E. Blay-Carreras (estel.blay@upc.edu)

Published by Copernicus Publications on behalf of the European Geosciences Union.

Abstract

Observations, mixed-layer theory and the Dutch Large-Eddy Simulation model (DALES) are used to analyze the dynamics of the boundary layer during an intensive operational period (1 July 2011) of the Boundary Layer Late Afternoon and Sunset Turbulence campaign. Continuous measurements made by remote sensing and in situ instruments in combination with radio soundings, and measurements done by remotely piloted airplane systems and two aircrafts probed the vertical structure and the temporal evolution of the boundary layer during the campaign. The initial vertical profiles of potential temperature, specific humidity and wind, and the temporal evolution of the surface heat and moisture fluxes prescribed in the numerical simulations are inspired by some of these observations.

The research focuses on the role played by the residual layer during the morning transition and by the large-scale subsidence on the evolution of the boundary layer. By using DALES, we show the importance of the dynamics of the boundary layer during the previous night in the development of the boundary layer at the morning. DALES numerical experiments including the residual layer are capable to model the observed sudden increase of the boundary-layer depth during the morning transition and the subsequent evolution of the boundary layer. The simulation shows a large increase of the entrainment buoyancy heat flux when the residual layer is incorporated into the mixed layer. We also examine how the inclusion of the residual layer above a shallow convective boundary layer modifies the turbulent kinetic energy budget.

Large-scale subsidence mainly acts when the boundary layer is fully developed and, for the studied day, it is necessary to be considered to reproduce the afternoon observations.

Additionally, we investigate how carbon dioxide (CO_2) mixing ratio stored the previous night in the residual layer plays a fundamental role in the evolution of the CO_2 mixing ratio during the following day.

ACPD

13, 31527–31562, 2013

1 Introduction

The atmospheric boundary layer, characterized by a clear diurnal cycle, has been intensively studied since the 70's. During the day with fair weather conditions a convective boundary layer (CBL) exists. The processes associated to the CBL development have been extensively studied. Sorbjan (1996), Sullivan et al. (1998) and Conzemius and Fedorovich (2006) studied the role of the entrainment processes, Moeng and Sullivan (1994), Fedorovich et al. (2001), Fedorovich et al. (2001), Pino et al. (2003), Pino et al. (2006a) and Pino and Vilà-Guerau de Arellano (2008) the contribution of shear in the generation and maintenance of CBL. Moreover, Yi et al. (2001), de Arellano et al. (2004), Casso-Torralba et al. (2008) and Vilà-Guerau de Arellano et al. (2009) studied the influence of CBL evolution on the carbon dioxide (CO_2) or isoprenes budget.

Several methodologies have been used to study the CBL: Large-Eddy Simulation numerical experiments (Moeng, 1984; Nieuwstadt and Brost, 1986; Cuijpers and Duynkerke, 1993; Sorbjan, 2007), mixed-layer model (MLM) (Tennekes, 1973; Tennekes and Driedonks, 1981; Fedorovich, 1995; Pino et al., 2006a), observations (Kaimal et al., 1976; Angevine et al., 1994; Cohn and Angevine, 2000) or laboratory experiments (Deardorff et al., 1980; Fedorovich et al., 1996).

During the night, a shallower stable boundary layer (SBL) with less turbulence intensity exists near the surface (Nieuwstadt, 1984; Carlson and Stull, 1986; Mahrt, 1998; Beare et al., 2006). Between this layer and the free atmosphere (FA), there may exist a neutrally stratified layer resulting from the decay of turbulence of the previous day CBL. This layer, called the residual layer (RL), appears before sunset, when eddies have less energy due to the reduction of surface fluxes. The RL has the same characteristics in the state variables as in the original CBL (Stull, 1988). The importance and the role of the RL was studied by some authors (Balsley et al., 2007; Wehner et al., 2010) who examined turbulence in the RL by analyzing the Richardson number gradient or to explain aerosol formation. Emeis and Schäfer (2006) by using different

ACPD
13, 31527–31562, 2013

instruments (e.g. sodar and ceilometer) measured and studied the heights of RL, CBL and SBL and their influence on urban air quality and pollution.

The evolution from CBL to SBL and vice versa happens through two transitional processes. These two periods are difficult to study due to their rapid variability. The afternoon transition has been studied by using observations or/and numerical simulations (Sorbjan, 1997; Cole and Fernando, 1998; Edwards et al., 2006; Pino et al., 2006a; Angevine, 2007; Nadeau et al., 2011). However, there are still many unknowns during this period: the presence of significant vertical movements in late afternoon, which appear even with very small surface heat flux, the influence of boundary layer processes in the turbulence decay, or what are the processes that govern the decrease of the boundary-layer depth (Lothon et al., 2012).

Regarding the morning transition, Angevine et al. (2001), Lapworth (2006), Bange et al. (2006) and Angevine (2007) investigated by using observations the timing and importance of entrainment and surface winds in the development of CBL. LeMone et al. (2002) analyzed data recorded during CASES-97 to study the warming and moistening of the atmosphere due to boundary-layer depth, wind direction, and surface heterogeneity during this period. Other authors (Sorbjan, 1996; Beare, 2008) analyzed the morning transition by using numerical models, such as Large-Eddy Simulation model (LES), to study the relevance of different temperature lapse rate or the importance of domain sizes and grid length or by using MLM to study the impact of the atmospheric boundary layer dynamics on the atmospheric chemistry (Ouwersloot et al., 2012).

Some aspects about the relevance of the RL during the morning transition have been studied by Fochesatto et al. (2001) and Gibert et al. (2011), who analyzed the dynamical coupling between the CBL and the RL by using lidar measurements. They observed the generation of internal gravity waves when there is an stable and stratified RL or when there is a thermal forcing. They concluded that horizontal wind shear is not enough to observe internal gravity waves. Other authors (Stensrud, 1993; Balin et al., 2004) focused their research on the elevated RL which is created when a CBL over an elevated terrain is advected over a lower CBL. Moreover, Han et al. (2011) studied the

ACPD
13, 31527–31562, 2013

evolution of the CBL when it is covered by a neutral layer after the morning transition. Finally, Doran et al. (2003) and Morris et al. (2010) examined the vertical mixing of different chemical compounds, such as ozone, nitrogen oxide or carbon monoxide during the morning transition.

Here the role of the RL during the morning transition and the role of subsidence during the whole evolution of the convective boundary layer is studied by using observations, mixed-layer theory (Tennekes and Driedonks, 1981) and the Dutch Large-Eddy Simulation model (DALES, Heus et al., 2010). In contrast with previous studies, by performing a sensitivity analysis on the residual layer and subsidence characteristics, we analyze the importance of these processes on the diurnal evolution of the convective boundary layer. Specifically, our research objectives can be summarized as follows:

1. To study the variations in the evolution of the boundary-layer depth due to the presence of RL and subsidence.
2. To analyze the relevance of considering the characteristics of the previous night in the potential temperature vertical profile and temporal evolution.
3. To observe the sensitivity of turbulent kinetic energy budget during morning transition and the evolution during the day due to RL.
4. To define the influence of RL on the observed evolution of the CO_2 mixing ratio.

We take profit of the observations taken during an intensive observational campaign of the project Boundary-Layer Late Afternoon and Sunset Turbulence (BLLAST, Lothon et al., 2012). During intensive operational periods (IOPs), more than 30 different instruments provided in situ (9 eddy covariance (EC) stations, towers, balloons, remote piloted aircraft systems and manned airplanes) and remote sensing (LIDAR, wind profiler) measurements.

The paper is structured as follows. In Sect. 2, we explain the main characteristics of the field campaign and the instruments selected for this study. Moreover, the numerical setup used in the models is also described in this section. Section 3 shows the

ACPD
13, 31527–31562, 2013

results focusing on the evolution of the boundary-layer depth, potential temperature, and turbulent kinetic energy budget to perform the sensitivity analysis. Furthermore, this section analyze the influence of RL on the observed evolution of the CO_2 mixing ratio. Finally, Sect. 4 summarizes the results.

2 Methodology

2.1 Observations

The observations used here to initialize, drive and qualitatively validate the numerical experiments were recorded during the observational campaign of the BLLAST project (Lothon et al., 2012), from 14 June to 8 July 2011 at Lannemezan (southern France). The main objective of this project is to study the structure and evolution of the boundary layer during the late afternoon transition.

During the whole campaign, UHF wind profiler measured vertical velocity with a vertical resolution of 150 m. In a $10 \times 10\,km^2$ area, EC stations located over different vegetation coverages (short and long grass, wheat and at the edge between long grass and wheat) measured with 10 Hz frequency acquisition the three wind components, the temperature, the specific humidity and the CO_2 concentration. Particularly, a 60 m tower had EC instruments at 30, 45 and 60 m. Heat, momentum and CO_2 fluxes at surface where estimated at all sites using a uniform processing method (De Coster and Pietersen, 2011).

Among the 19 radiosondes launched between 01:30 UTC to 23:00 UTC on the IOP under study (1 July 2011) we use the ones launched over our area of interest, where the fluxes were measured.

2.2 Numerical experiments

Two numerical models of different complexity have been used to study the evolution of the convective boundary layer during the selected day: DALES (Heus et al., 2010)

ACPD
13, 31527–31562, 2013

and a mixed-layer model (MLM, Tennekes and Driedonks, 1981). Both models were initialized and driven by observations. Specifically, for all the numerical experiments performed with both models, the same evolution of the surface sensible and latent heat fluxes was prescribed based on the average of the observed fluxes recorded by EC instruments over different land uses.

The domain chosen for the DALES simulations has $12.8 \times 12.8 \times 3\,\mathrm{km}^3$, and 256 points are defined in each direction. This setup has a similar horizontal domain to the campaign site, having also enough vertical resolution to study entrainment processes. Our DALES numerical experiments during 12.5 h starting at 07:30 UTC, to include the morning transition in the simulation.

To analyze the role played by the RL in the morning evolution of the convective boundary layer, two different vertical profiles of potential temperature (θ) and specific humidity (q) are considered to initialize DALES. To include the residual layer in DALES (RL numerical experiments), we initialize it by following the observations taken by the radio sounding launched at 07:30 UTC. Figure 1 shows the vertical profile of θ and q observed at 07:30 UTC and the prescribed vertical profiles used for initializing DALES RL and no-RL numerical experiments.

Table 1 shows the values of the potential temperature, specific humidity and horizontal wind components that define the initial profiles of the DALES and MLM numerical experiments. For the RL numerical experiments, the initial vertical profiles of θ and q are divided in three different layers: CBL from surface to $z_{1,0}$, RL from $z_{1,0}$ to $z_{\mathrm{RL},0}$, and FA above $z_{\mathrm{RL},0}$. The potential temperature (specific humidity) in the CBL and in the RL are, respectively, $\theta_{1,0}$ ($q_{1,0}$) and $\theta_{\mathrm{RL},0}$ ($q_{\mathrm{RL},0}$). The inversion jumps at the two boundaries are $\Delta\theta_{1,0}$ ($\Delta q_{1,0}$) and $\Delta\theta_{\mathrm{RL},0}$ ($\Delta q_{\mathrm{RL},0}$). In the FA, the potential temperature (specific humidity) lapse rate is γ_θ (γ_q).

For the numerical experiments without the residual layer (nRL) the initial vertical profiles for DALES (Fig. 1) are divided in two layers: CBL and FA, and the same notation is used for the CBL values ($\theta_{1,0}$ and $q_{1,0}$) and FA lapse rates (γ_θ and γ_q), being $z_{1,0}$ the initial boundary-layer depth.

ACPD
13, 31527–31562, 2013

LeMone et al. (1999); Pino et al. (2003); Conzemius and Fedorovich (2006), among others showed that shear at the inversion influences entrainment fluxes. Consequently, initial and geostrophic vertical profiles are defined for all the DALES numerical experiments based on the radio sounding observations. Constant with height geostrophic wind is considered ($u_g = 10$, $v_g = 0\,\mathrm{m\,s^{-1}}$). The initial wind profile is constant with height below the FA, $u = -2.95$, $v = 0.52\,\mathrm{m\,s^{-1}}$, being equal to the geostrophic wind in the FA.

To study the role of subsidence, additional simulations are performed. The value of subsidence to be included in DALES and MLM numerical experiments are obtained, following Yi et al. (2001), by analyzing the observed vertical profile of the potential temperature at 01:30 and 07:30 UTC on 1 July 2011 (see Fig. 1). The depth of the residual layer (z_{RL}) decreases 215 m within 6 h (01:30–07:30 UTC). This represents a subsidence velocity of $9.95 \times 10^{-3}\,\mathrm{m\,s^{-1}}$. Subsidence is included in two DALES numerical experiments as follows. Subsidence vertical profile increases linearly from 0 at the surface to $9.95 \times 10^{-3}\,\mathrm{m\,s^{-1}}$ at $z_{RL,0}$ in both numerical experiments (RLs and nRLs numerical experiments). In FA, the subsidence is constant equal to $9.95 \times 10^{-3}\,\mathrm{m\,s^{-1}}$. Despite subsidence may evolve during the day, we prescribe a constant subsidence profile because the main objective of the paper is not exactly fit the observations but to analyze the role of RL and subsidence. For this same reason, and taking into account the low winds recorded during the selected IOP, heat and moisture advection are not considered.

By combining RL and subsidence, four different DALES numerical experiments were performed: RL with subsidence (RLs), RL without subsidence (RLns), no-RL with subsidence (nRLs) and no-RL without subsidence (nRLns).

MLM is used to create fast and simple characterization of the CBL and the results can be contrasted with the results of DALES numerical experiments to verify if simple models can also simulate the evolution of the CBL from midday considering subsidence. The version used here of the MLM does not include the RL in its vertical profile. Consequently, it can only be used for developed convective boundary layers. To initialize MLM, we used the information of the first radio sounding which shows a completely

ACPD
13, 31527–31562, 2013

developed CBL; the one launched at 11:00 UTC. Table 1 shows the values which characterize the MLM initial profile of θ and q. We prescribed in MLM a divergence at $z_{1,0}$, being equal to 7.65×10^{-6} s^{-1}, obtained by considering the subsidence velocity equal to 9.95×10^{-3} m s^{-1} and the initial depth of the boundary-layer for MLM ($z_{1,0}$ = 1300 m).

3 Results

The study is focused on 1 July 2011, that was the second of a three consecutive IOPs with increasingly high temperatures. During this IOP, a large high pressure system was located southwest of the British Islands. The influence of this high pressure system extends towards the east. This results at the BLLAST site in clear skies, fair weather, and weak wind coming from the north turning to the east during the day at low levels. Higher up in the atmosphere, at 500 hPa, a strong ridge extends over southern Europe causing a predominantly western flow in the region.

In the next sections, we demonstrate the importance of RL during the morning transition and of subsidence during the afternoon by analyzing the observed and simulated evolution of the boundary-layer depth, potential temperature, turbulent kinetic energy budget and its influence on the evolution of CO_2.

3.1 Mixed-layer potential temperature temporal evolution

Figure 2 shows the temporal evolution of potential temperature obtained by the MLM with subsidence and obtained by the four DALES numerical experiments in the middle point between the surface and the height when the surface heat flux becomes 0 W m^{-2} ($z_0 < z_1$). The figure also shows the observed temporal evolution of the 2 m potential temperature over different land uses during 1 July 2011. Differences between potential temperature measurements are below 1 K except for the potential temperature measured over wheat. As it was already pointed out by previous studies (Nadeau et al. (2011), among others), surface heat flux over wheat is larger yielding to larger 2 m

ACPD
13, 31527–31562, 2013

potential temperature. Notice that measurement height is different to the height where DALES results are considered, what may produce some discrepancies.

By using mixed-layer theory, if heat advection is considered negligible due to the low winds recorded, the time evolution of the mean potential temperature in the mixed layer ($\overline{\theta}$) in convective conditions is driven by surface and entrainment heat fluxes, and reads (Tennekes and Driedonks, 1981):

$$\frac{\partial \overline{\theta}}{\partial t} = \frac{\overline{w'\theta'}|_s - \overline{w'\theta'}|_1}{z_1}, \quad (1)$$

where $\overline{w'\theta'}|_s$ and $\overline{w'\theta'}|_1$ are the turbulent heat flux at the surface and at z_1 (entrainment heat flux), respectively. Taking into account that the surface heat flux is the same for all the numerical experiments, the difference in the evolution of potential temperature between the numerical experiments is explained by entrainment heat flux and z_1 differences.

If large-scale subsidence is not considered, zeroth-order mixed-layer theory postulates that entrainment heat flux reads (Lilly, 1968; Tennekes, 1973; Tennekes and Driedonks, 1981; Carson, 1973):

$$\overline{w'\theta'}|_1 = -\Delta\theta_1 \frac{\partial z_1}{\partial t}, \quad (2)$$

where $\Delta\theta_1$ is the jump of the potential temperature at the inversion.

If the residual layer is not considered (nRLs and nRLns numerical experiments), the simulated 2 m potential temperature increases rapidly due to the initially prescribed large potential temperature jump, which increases the entrainment heat flux. Moreover, the CBL is shallow during the morning enhancing the CBL-heating rate (see Eqs. 1 and 2). Consequently, these DALES numerical experiments do not fit the observations.

On the contrary, if the residual layer is included in the initial profile of DALES numerical experiments, the temporal evolution of mixed-layer potential temperature presents

ACPD
13, 31527–31562, 2013

two different regimes. For approximately the first 1.5 h of the simulation, the boundary layer is shallow but the inversion layer jump is moderate when compared with the nRL numerical experiments. Consequently, entrainment heat flux is smaller and potential temperature increases smoothly, approximately fitting the observations. At 09:00 UTC, when the potential temperature in the mixed layer and in the residual layer are the same, the boundary-layer depth increases approximately to 1300 m. Although, the new potential temperature inversion jump is larger, the heating rate is lower compared with the first 1.5 h of simulation due to the large z_1 simulated at this moment, and DALES RL numerical experiments fit better the observations.

Once the mixed layer has incorporated the residual layer, MLM starting at 11:00 UTC, simulates correctly the evolution of the potential temperature, being close to the observed values and to the results of DALES numerical experiments that take into account the residual layer.

The role played by subsidence in the evolution of the potential temperature can be only appreciated at the end of the afternoon, when the boundary layer growth is small. However, none of the numerical experiments is able to simulate the decrease of potential temperature observed from 17:00 UTC which maybe is produced by a weak negative heat advection due to the change in wind direction produced by slope flows.

3.2 Boundary-layer depth temporal evolution

Figure 3 shows the time evolution of the refractive structure coefficient (CN2) observed by the UHF wind profiler and the boundary layer depth estimated from the radio soundings launched at 07:30, 11:00, 14:00, 17:00, and 20:00 UTC, and obtained by MLM with subsidence and by DALES numerical experiments (RLs, RL, nRLs and nRL). z_1 for MLM and DALES is defined as the height where the minimum buoyancy flux occurs (Seibert et al., 2000). z_1 obtained from the radio sounding data is defined as the height where the maximum virtual potential temperature gradient occurs. The reliability to obtain the depth of the boundary layer by using isolated radio soundings has been sometimes criticized (e.g. Stull, 1988). Nevertheless, radio sounding measurements in

ACPD
13, 31527–31562, 2013

this study fit correctly with the UHF measurements and the small dissimilarities can be attributed to the different procedures used to obtain z_1 (Sullivan et al., 1998).

UHF wind profiler measurements show the existence of a residual layer during the early morning and how around 09:00 UTC the mixed layer merges with the RL from the previous night producing a sudden increase of the boundary-layer depth (see Fig. 3). From this moment, the observed boundary-layer depth remains approximately constant during 7 h. Taking into account that surface heat flux is still positive for several hours, this might be explained due to the existence of subsidence that prevents the mixed layer to grow. During the afternoon, due to subsidence and the decrease of surface fluxes, UHF and radio sounding measurements show a slight decrease of the boundary-layer depth from 17:00 UTC.

DALES numerical experiments including the residual layer in its initial profile fit correctly the observations, simulating the sudden increase of the boundary-layer depth during the morning transition. On the other hand, DALES nRL numerical experiments simulate a progressive increase of the boundary-layer depth and underestimate by several hundred meters the observations during the whole morning, until 13:00 UTC. In all DALES results, small fluctuations on z_1 are observed at the end of the day (around 18:00 UTC) due to cease of the surface heat flux which produces fluctuations on the buoyancy heat flux vertical profile (Pino et al., 2006b).

Previous studies such as Fedorovich (1995) demonstrate that zeroth-order models can be also useful and valid to develop studies of the evolution of the boundary-layer. In our study, the boundary-layer depth obtained with MLM has almost the same value as in DALES numerical experiments that include both the residual layer and subsidence confirming the studies previously developed.

Regarding the role of subsidence in the numerical experiments, it can be observed that the numerical experiments that include subsidence (RLs, nRLs, MLM) fit better with the observations but slightly underestimate the observed boundary-layer depth (less than 100 m with respect UHF measurements) maybe due to subsidence diurnal variability. The numerical experiments that do not consider subsidence overestimate the

ACPD
13, 31527–31562, 2013

observed z_1 by less than 200 m. Long-term observations of the boundary-layer show the importance to consider subsidence to obtain realistic approximations (Yi et al., 2001; H. Pietersen personal communication, 2013).

3.3 Potential temperature vertical profile

Figure 4 shows the vertical profile of potential temperature observed with the radio soundings, obtained by MLM including subsidence, and obtained by DALES numerical experiments at different hours on 1 July 2011. The figure illustrates the importance of the morning conditions on the evolution of the boundary-layer depth and of the potential temperature during the whole day. At 08:30 UTC (Fig. 4a), when the RL has not been already incorporated into the boundary layer, mixed-layer potential temperature in the numerical experiments which consider the RL are 1.7 K lower than nRL numerical experiments, even though the boundary-layer depth is similar, due to the larger potential temperature inversion jump simulated by the nRL numerical experiments. As day progresses, the difference of mixed-layer θ increases between nRL and RL numerical experiments; RL numerical experiments become approximately 4 K lower than nRL numerical experiments (see Fig. 4b) fitting the observations. However, after 13:00 UTC when the boundary-layer depth simulated by the nRL numerical experiments reaches around 1300 m, the difference in the mixed-layer potential temperature between RL and nRL numerical experiments is maintained (see Fig. 4c and d) due to the similar values of entrainment heat flux and boundary layer depth simulated for all the numerical experiments. Moreover, the influence of subsidence in the boundary-layer depth and potential temperature is noticeable from midday. RLns and nRLns clearly overestimate the observed boundary-layer depth by several hundred meters and the potential temperature is 0.5 K colder (see Fig. 4b and c).

To understand the differences in the potential temperature vertical profile between the numerical experiments during the morning, as the surface heat flux are the same, we focus our analysis on the entrainment heat flux and on the boundary-layer depth (see Eq. 1). Figure 5 shows the early morning temporal evolution of heat flux at z_1 for

ACPD
13, 31527–31562, 2013

the nRLns and RLns numerical experiments. Several authors (Sorbjan, 1996; Sullivan et al., 1998; Conzemius and Fedorovich, 2006), pointed out the importance of the entrainment processes for the evolution of the potential temperature. During the early morning (before 09:00 UTC) z_1-growth is similar in both simulations. Consequently, the difference of the entrainment heat flux between the numerical experiments is due to the potential temperature inversion jump (see Eq. 2); $\Delta\theta_1$ is 2 K larger for nRLns than for RLns at 08:30 UTC (see Fig. 4a). Therefore, larger entrainment heat flux is obtained for the nRLns numerical experiment and the mixed-layer potential temperature increases.

When the residual layer is incorporated into the boundary layer in the RLns numerical experiment, entrainment heat flux changes suddenly from -0.02 to $-0.045\,\mathrm{K\,m\,s^{-1}}$, introducing more air from the FA mainly due to the increase of the potential temperature inversion jump (from nearly 0 to 1 K) and also by the large increase in the z_1-growth. From this moment to the end of the simulation, entrainment heat fluxes for both DALES numerical experiments remain close due to the similar boundary-layer growth and potential temperature inversion jumps.

3.4 Turbulent kinetic energy budget

Under horizontally homogeneous conditions, the turbulent kinetic energy (TKE) budget reads (Stull, 1988):

$$\frac{\partial \overline{e}}{\partial t} = -\left[\overline{u'w'}\frac{\partial u}{\partial z} + \overline{v'w'}\frac{\partial u}{\partial z}\right] + \frac{g}{\theta_{\mathrm{vr}}}\overline{w'\theta'_v} - \frac{\partial \overline{w'e'}}{\partial z} - \frac{1}{\rho_0}\frac{\partial \overline{w'p'}}{\partial z} - \varepsilon \qquad (3)$$

where u', v', w' are the turbulent fluctuations of the velocity components, p is the pressure, ρ_0 is a reference density, θ_{vr} is a reference virtual potential temperature, $\overline{e} = 0.5(\overline{u'^2 + v'^2 + w'^2})$ is the mean turbulent kinetic energy and ε is the viscous dissipation of TKE. The term on the left-hand side represents storage (STO) of TKE, and the terms on the right-hand side represent shear (S), and buoyancy production (B), turbulent transport (T), pressure correlation (P), and viscous dissipation (D) terms.

ACPD
13, 31527–31562, 2013

TKE budget was analyzed during the entire diurnal cycle but firstly we focus during the morning because we want to analyze TKE variations when the RL is incorporated in the CBL. Figure 6 shows the vertical profile averaged every 30 min of the different resolved TKE terms at (top) 08:30, (middle) 09:00, and (bottom) 14:00 UTC, for (left panels) RLns and (right panels) nRLns DALES numerical experiments. Notice the different range of the horizontal axis of some of the plots. The turbulent transport and the pressure correlation terms are plotted together as the convergence of the turbulence kinetic energy flux (Driedonks, 1982).

At 08:30 UTC (see Fig. 6a and d), when the boundary layer is shallow for both numerical experiments, larger values of B and S terms at z_1 are obtained for the nRLns numerical experiment. This is due to the higher entrainment heat and momentum fluxes at z_1. To balance the budget, the pressure-transport term and the dissipation term are also larger for the nRLns numerical experiment, especially in the entrainment zone. The TKE distribution of Fig. 6a and d was previously observed in the LES morning transition analysis by Beare (2008). Moreover, in Fig. 6a at the top of the RL, S is present due to the interaction between this layer and the FA which have different wind conditions.

The effect of the inclusion of the residual layer into the mixed layer between 08:30 and 09:00 UTC can be clearly seen by comparing Fig. 6a and b, where the TKE terms of the RLns numerical experiment are represented. Storage, shear and dissipation terms become approximately constant in the middle of the boundary layer, with the three terms larger at the inversion due to the larger potential temperature inversion jump. Consequently, the pressure-transport term increases in this zone.

From 08:30 to 09:00 UTC, the value of TKE terms for the nRLns numerical experiment (see Fig. 6d and e) decreases. This is due to the increase of boundary-layer depth and the reduction of the inversion strength that primarily reduces buoyancy and shear term at the inversion and, to balance the budget, the other terms.

At 14:00 UTC (Fig. 6c and f), when similar z_1 is simulated for both numerical experiments (see Fig. 3), STO, B and T+P terms are similar for both numerical experiments

ACPD
13, 31527–31562, 2013

but larger S and, consequently D, terms are found for the RLns numerical experiment near the surface. This is due to the fact that, from midday, when the boundary layer is similar for both numerical experiment, larger surface momentum fluxes are obtained for RLns due to the larger mixed-layer winds (especially v) simulated by this numerical experiment.

Figure 7 shows the vertical integration of each TKE-term from the surface up to z_1 normalized by z_1. For both RLns and nRLns numerical experiments, STO and T+P terms remain small when comparing with the other terms during the whole evolution, being negligible after the morning transition. Before the inclusion of the RL, which can be clearly seen by the maximum of B-integrated term around 09:00 UTC, RLns numerical experiment presents very small integrated-S term due to the low z_1 and the small wind shear existing at the surface and inversion zone. On the contrary, integrated-B is larger when comparing with nRLns numerical experiment because for this last numerical experiment much larger entrainment negative heat flux are simulated, producing a smaller vertically integrated-B (see Fig. 6a and c). As a consequence, integrated-D is slightly smaller for the RLns numerical experiments before 09:30 UTC. From this moment, the vertically integrated-S term increases for the RLns numerical experiment because the integration covers a larger vertical domain, and it decreases for nRL because wind shear decreases at the inversion and z_1 growth rate is not enough to compensate it. Until 11:00 UTC, the integrated-B term increases for both numerical experiments (surface and entrainment heat flux increase), becoming similar. Therefore, integrated-D remains almost constant for nRLns but increases for RLns. At approximately 11:00 UTC, the vertically integrated-S and D terms are similar for both numerical experiments.

From 11:00 UTC the vertically integrated-B term is similar for both numerical experiment because despite z_1 are different until 15:00 UTC (see Fig. 3), and consequently larger positive and negative heat fluxes are simulated for the nRLns numerical experiment, its integration produces similar values. However, the vertically integrated-S term decreases for the nRLns numerical experiment but continuously increases until

ACPD
13, 31527–31562, 2013

15:00 UTC for RLns, mainly due to the larger wind shear at the surface. Consequently, to balance the TKE budget, larger vertically integrated-D is also obtained for the RLns numerical experiment.

3.5 Influence of the residual layer on the observed evolution of the CO_2 mixing ratio

In this section, we analyze the importance of entrainment and surface CO_2 fluxes measured over different land uses in the evolution of the CO_2 mixing ratio. Some authors (de Arellano et al., 2004; Casso-Torralba et al., 2008) have analyzed the importance of entrainment CO_2 fluxes, that are especially relevant during early morning, but over homogenous terrains. Moreover, Moncrieff et al. (1997), Baldocchi et al. (1998) and Soegaard (1999) analyzed the evolution of the CO_2 mixing ratio over heterogeneous terrains during daily and longer periods of time. Here, we deal with CO_2 surface fluxes measured over different land uses and what is their influence on CO_2 mixing ratio in an evolving convective boundary layer.

Figure 8 shows the observed temporal evolution from 14:00 UTC on 30 June 2011 to 14:00 UTC on 1 July 2011 of the CO_2 mixing ratio and CO_2 flux measured at 2 m over different land uses (moor, corn and grass). As a reference, it is also included the measurements taken by the 30 m EC sensor located at the 60 m tower over grass. Differences between CO_2 mixing ratio measurements over different land uses on 1 July 2011 are below 2 ppm during daytime and below 10 ppm during nighttime. By comparing 2 and 30 m measurements, differences of CO_2 mixing ratio are below 2 ppm at nighttime and below 12 ppm during daytime. In general during the night, larger CO_2 mixing ratio is observed near the surface than at 30 m over the same land use. Due to the large fluctuations of the measurements this fact cannot be corroborated.

Between 05:00 and 09:00 UTC, a remarkable decrease of the CO_2 mixing ratio is observed at 2 m. At 30 m the decrease in CO_2 is less pronounced. Before 09:00 UTC, boundary layer is shallow (see Fig. 3), and the RL has not been incorporated yet to the mixed layer. During these hours surface uptake and mainly CO_2 entrainment flux drive

ACPD
13, 31527–31562, 2013

the decrease of CO_2 mixing ratio (de Arellano et al., 2004; Casso-Torralba et al., 2008). Additionally, during early morning advection may also play a role. When entrainment flux mainly drives the decrease of CO_2 mixing ratio (around 06:00 UTC) the decrease is similar at both heights. Later on, when CO_2 surface fluxes become larger, differences appear between the CO_2 at 2 m and at 30 m. At 30 m, as expected the CO_2 surface flux is smaller, and consequently, there is a smother decrease of the CO_2 mixing ratio at this altitude.

During this IOP, no measurements of CO_2 entrainment flux were taken. However, since we have measurements of CO_2 surface flux, boundary-layer depth and temporal evolution of the CO_2 mixing ratio, in convective conditions, CO_2 entrainment flux can be estimated. By neglecting CO_2 advection and mean vertical velocity, the storage of CO_2 mixing ratio in the mixed layer reads:

$$\frac{\partial \overline{c}}{\partial t} = \frac{\overline{w'c'}|_s - \overline{w'c'}|_1}{z_1}, \quad (4)$$

where $\overline{w'c'}|_s$ and $\overline{w'c'}|_1$ are the turbulent CO_2 flux at the surface and at z_1 (CO_2 entrainment flux), respectively and $\overline{c}$ is the mean CO_2 mixing ratio in the mixed layer. By using Eq. (4), it can be calculated that CO_2 entrainment flux is 3 times larger than CO_2 surface flux before 09:00 UTC.

Once the RL is incorporated into the mixed layer, the boundary-layer depth increases suddenly to values close to 1300 m (see Fig. 3). As it was shown in Sect. 3.2, the boundary-layer growth is almost zero from that time. Therefore, CO_2 entrainment flux is almost negligible (Yi et al., 2001). After 09:00 UTC, it can be observed in Fig. 8a that CO_2 mixing ratio is around 297 ppm over all the surfaces, varying between 1 and 1.5 ppm, depending on the land use, during 3 h. However, clearer differences in the CO_2 surface fluxes are observed (see Fig. 8b). CO_2 mixing ratio present only slight variations because the observed z_1 from 09:00 UTC is large, and consequently $\overline{w'c'}|_s/z_1$ is small. For the land uses shown in Fig. 8, $\partial C/\partial t$ is around 0.3 ppm h^{-1} for moor and wheat, and close to 0.5 ppm h^{-1} for corn. Therefore, the mixing ratio is controlled

ACPD
13, 31527–31562, 2013

almost by mixed layer growth, with the surface flux playing not an important role (Culf, 1997; Pino et al., 2012).

From this analysis, we conclude that on 1 July 2011, before the merging of CBL and RL, CO_2 mixing ratio decreases from the high values of CO_2 observed during the night to the CO_2 mixing ratio of RL (CO_2 mixing ratio of the previous day) mainly due to CO_2 entrainment flux. This CO_2 mixing ratio is almost constant during the rest of the day due to the large and constant value of z_1.

4 Conclusions

The impact of the residual layer and subsidence on the evolution of a CBL is studied by means of observations taken during the BLLAST campaign, DALES numerical experiments and mixed-layer theory. In contrast with previous analysis of the morning transition (e.g. Angevine et al., 2001; LeMone et al., 2002; Lapworth, 2006; Beare, 2008), we use a sensitivity analysis of the the numerical experiments to study the influence of the two processes in the evolution of the convective boundary layer.

Depending on whether residual layer is considered or not in the DALES numerical experiments, different evolutions of the boundary layer are simulated. Potential temperature simulated by the numerical experiments considering the residual layer fits correctly the observations in contrast with numerical experiments without residual layer (nRL) which simulate a too large mixed-layer heating rate during the early morning. By using mixed-layer theory, we conclude that the difference in the evolution of the potential temperature is due to entrainment heat flux, because the same surface fluxes are prescribed for all the numerical experiments and the z_1 growth is similar before the morning transition. After the merge of residual layer and CBL, large entrainment heat flux is simulated in the numerical experiments with residual layer because $\Delta\theta_1$ and $\partial z_1/\partial t$ also increase.

For DALES numerical experiments including residual layer, a rapid increase of boundary-layer depth is obtained, similar to observations, when the residual layer is

ACPD
13, 31527–31562, 2013

incorporated in the mixed layer. In contrast, boundary-layer depth for the numerical experiments without residual layer grows at a lower rate, underestimating it relatively to the observations by several hundred meters until 13:00 UTC.

Subsidence also plays an important role in the evolution of the CBL. Without subsidence included in the simulations, the simulated boundary layer depth continues to grow reaching higher values than the observed. Moreover, different initializations of subsidence are compared: DALES with a simple vertical profile and MLM with a subsidence value defined at the top of the CBL. The evolution of the boundary-layer depths are similar with both initializations, and in agreement with the observations verifying the practicality and effectiveness of simpler models.

DALES allows us to evaluate the influence of the residual layer in the TKE budget during the morning (08:30–09:00 UTC). When the residual layer is taken into account buoyancy, transport-pressure and dissipation are the largest terms before the inclusion of the residual layer. When it is incorporated into the mixed-layer, buoyancy and shear increases at the inversion and near the surface. On the contrary, if residual layer is not considered TKE terms present the typical evolution during boundary layer growth (Pino and Vilà-Guerau de Arellano, 2008). Regarding the vertical integration of the TKE-terms, the differences between the numerical experiments with or without residual layer are mainly due to the shear term. Much larger winds are simulated for the RL numerical experiments and consequently larger shear are obtained for this numerical experiment, especially at the surface.

We also analyze the influence of the residual layer in the evolution of CO_2 mixing ratio by using the observations. Before 09:00 UTC, CO_2 surface fluxes are small, the boundary layer is shallow, and CO_2 mixing ratio decrease is mainly driven by CO_2 entrainment flux. After the inclusion of the residual layer into the mixed layer, the boundary layer depth is almost constant during the rest of the day. Therefore CO_2 entrainment flux is very small and, despite the larger observed CO_2 surface flux observed over some surfaces, the CO_2 mixing ratio is very similar over the different land uses. This is

ACPD
13, 31527–31562, 2013

due because storage term is below 0.5 ppm h^{-1} over all the surfaces due to the large value of z_1.

We can conclude that a precise definition of the characteristics of the residual layer is fundamental, even though it is complex because the evolution of the main variables in the residual layer during the previous night depends on different factors such as advection or subsidence which can change in time.

Acknowledgements. This work was supported by Spanish MINECO projects CGL2009-08609, and CGL2012-37416-C04-03. DALES simulations were performed at SARA with the financial support of the project NCF-NWO SH-060-09. The MODEM radio sounding station and the UHF wind profiler have been supported by CNRS, Université Paul Sabatier and FEDER program (Contract num. #34172-Development of the instrumentation of Observatoire Midi-Pirénées-PIRENEA-ESPOIR). The 60 m tower equipment has been supported by CNRS, Université Paul Sabatier and European POCTEFA 720 FluxPyr program. One EC station was supported by Wageningen University and two EC stations were supported by the University of Bonn and DFG project SCHU2350/21.

BLLAST field experiment was made possible thanks to the contribution of several institutions and supports: INSU-CNRS (Institut National des Sciences de l'Univers, Centre National de la Recherche Scientifique, LEFE-IDAO program), Météo-France, Observatoire Midi-Pirénées (University of Toulouse), EUFAR (EUropean Facility for Airborne Research) and COST ES0802 (European Cooperation in the field of Scientific and Technical). The field experiment would not have occurred without the contribution of all participating European and American research groups, which all have contributed in a significant amount. BLLAST field experiment was hosted by the instrumented site of Centre de Recherches Atmosphériques, Lannemezan, France (Observatoire Midi-Pirénées, Laboratoire d'Aérologie). BLLAST data are managed by SEDOO, from Observatoire Midi-Pirénées.

ACPD
13, 31527–31562, 2013

References

Angevine, W. M.: Transitional, entraining, cloudy, and coastal boundary layers, Acta Geophys., 56, 2–20, 2007. 31530

Angevine, W. M., White, A. B., and Avery, S. K.: Boundary-layer depth and entrainment zone characterization with a boundary-layer profiler, Bound.-Lay. Meteorol., 68, 375–385, 1994. 31529

Angevine, W. M., Baltink, H. K., and Bosveld, F. C.: Observations of the morning transition of the convective boundary layer, Bound.-Lay. Meteorol., 101, 209–227, 2001. 31530

Baldocchi, D. and Meyers, T.: On using eco-physiological, micrometeorological and biogeochemical theory to evaluate carbon dioxide, water vapor and trace gas fluxes over vegetation: a perspective, Agr. Forest Meteorol., 90, 1–25, 1998. 31543

Balin, I., Parlange, M., Calpini, B., Simeonov, V., and van den Bergh, H.: Elevated atmospheric boundary layer over the Swiss Alps during the August 2003 heat wave, in: 22nd Internation Laser Radar Conference, Matera, Italy, 12–16 July, ESA SP-561, http://adsabs.harvard.edu/full/2004ESASP.561..781B, 2004. 31530

Balsley, B. B., Svensson, G., and Tjernström, M.: On the scale-dependence of the gradient Richardson number in the residual layer, Bound.-Lay. Meteorol., 127, 57–72, 2007. 31529

Bange, J., Spieß, T., and van den Kroonenberg, A.: Characteristics of the early-morning shallow convective boundary layer from Helipod flights during STINHO-2, Theor. Appl. Climatol. 90, 113–126, 2006. 31530

Beare, R. J.: The role of shear in the morning transition boundary layer, Bound.-Lay. Meteorol., 129, 395–410, 2008. 31530, 31541

Beare, R. J., Edwards, J. M., and Lapworth, A. J.: Simulation of the observed evening transition and nocturnal boundary layers: large-eddy modelling, Q. J. Roy. Meteor. Soc., 132, 61–80, 2006. 31529

Carlson, M. A., and Stull, R.: Subsidence in the nocturnal boundary layer, J. Clim. Appl. Meteorol., 25, 1088–1099, 1986. 31529

Carson, D. J.: The development of a dry inversion-capped convectively unstable boundary layer, Q. J. Roy. Meteor. Soc., 99, 450–467, 1973. 31536

Casso-Torralba, P., Vilà-Guerau de Arellano, J., Bosveld, F. C., Soler, M. R., Vermeulen, A., Werner, C., and Moors, E.: Diurnal and vertical variability of the sensible heat and car-

ACPD
13, 31527–31562, 2013

bon dioxide budgets in the atmospheric surface layer, J. Geophys. Res., 113, D12119, doi:10.1029/2007JD009583, 2008. 31529, 31543, 31544
Cohn, S. A. and Angevine, W. M.: Boundary layer height and entrainment zone thickness measured by lidars and wind-profiling radars, J. Appl. Meteorol., 39, 1233–1247, 2000. 31529
Cole, G. S. and Fernando, H. J. S.: Some aspects of the decay of convective turbulence, Fluid Dyn. Res., 23, 161–176, 1998. 31530
Conzemius, R. J. and Fedorovich, E.: Dynamics of sheared convective boundary layer entrainment, Part 1: Methodological background and large-eddy simulations, J. Atmos. Sci., 63, 1151–1178, 2006. 31529, 31534, 31540
Culf, A. D., Fisch, G., Malhi, Y., and Nobre, C. A.: The influence of the atmospheric boundary layer on carbon dioxide concentrations over a tropical forest, Agr. Forest Meteorol., 85, 149–158, 1997. 31545
Cuijpers, J. W. M. and Duynkerke, P. G.: Large eddy simulation of trade wind cumulus clouds, J. Atmos. Sci., 50, 3894–3908, 1993. 31529
de Arellano, J. V.-G., Gioli, B., Miglietta, F., Jonker, H. J. J., Baltink, H. K., Hutjes, R. W. A., and Holtslag, A. A. M.: Entrainment process of carbon dioxide in the atmospheric boundary layer, J. Geophys. Res., 109, D18110, doi:10.1029/2004JD004725, 2004. 31529, 31543, 31544
De Coster, O. M. Y. and Pietersen, H. P.: BLLAST-uniform processing of Eddy-Covariance data, Internship Report Meteorology and Climatology, Wageningen University and Research Center, the Netherlands, 30 pp., Internship report, http://bllast.sedoo.fr/documents/reports/H-Pietersen_O-de-Coster_BLLAST-surf_flx-uniform-processing.pdf, 2011. 31532
Deardorff, J. W., Willis, G. E., and Stockton, B. H.: Laboratory studies of the entrainment zone of a convectively mixed layer, J. Fluid Mech., 100, 41–64, 1980. 31529
Doran, J. C., Berkowitz, C. M., Coulter, R. L., Shaw, W. J., and Spicer, C. W.: The 2001 Phoenix Sunrise experiment: vertical mixing and chemistry during the morning transition in Phoenix, Atmos. Environ., 37, 2365–2377, 2003. 31531
Driedonks, A. G. M.: Models and observations of the growth of the atmospheric boundary layer, Bound.-Lay. Meteorol., 23, 283–306, 1982. 31541
Edwards, J. M., Beare, R. J., and Lapworth, A. J.: Simulation of the observed evening transition and nocturnal boundary layers: Single-column modelling, Q. J. Roy. Meteor. Soc., 132, 61–80, 2006. 31530

ACPD
13, 31527–31562, 2013

Emeis, S. and Schäfer, K.: Remote sensing methods to investigate boundary-layer structures relevant to air pollution in cities, Bound.-Lay. Meteorol., 121, 377–385, 2006. 31529
Fedorovich, E.: Modeling the atmospheric convective boundary layer within a zero-order jump approach: an extended theoretical framework, J. Appl. Meteorol., 34, 1916–1928, 1995. 31529, 31538
Fedorovich, E., Kaiser, R., Rau, M., and Plate, E.: Wind tunnel study of turbulent flow structure in the convective boundary layer capped by a temperature inversion, J. Atmos. Sci., 53, 1273–1289, 1996. 31529
Fedorovich, E., Nieuwstadt, F. T. M., and Kaiser, R.: Numerical and laboratory study of a horizontally evolving convective boundary layer. Part 1: Transition regimes and development of the mixed layer, J. Atmos. Sci., 58, 70–86, 2001. 31529
Fochesatto, G. J., Drobinski, P., Flamant, C., Guedalia, D., Sarrat, C., Flamant, P. H., and Pelon, J.: Evidence of dynamical coupling between the residual layer and the developing convective boundary layer, Bound.-Lay. Meteorol., 99, 451–464, 2001. 31530
Garai, A., Pardyjak, E. R., Steeneveld, G.-J., and Kleissl, J.: Surface temperature and surface-layer turbulence in a convective boundary layer, Bound.-Lay. Meteorol., 148, 51–72, 2013.
Gibert, F., Arnault, N., Cuesta, J., Plougonven, R., and Flamant, P. H.: Internal gravity waves convectively forced in the atmospheric residual layer during the morning transition, Q. J. Roy. Meteor. Soc., 137, 1610–1624, 2011. 31530
Han, B., Lü, S., and Ao, Y.: Development of the convective boundary layer capping with a thick neutral layer in Badanjilin: observations and simulations, Adv. Atmos. Sci., 29, 177–192. 31530
Heus, T., van Heerwaarden, C. C., Jonker, H. J. J., Pier Siebesma, A., Axelsen, S., van den Dries, K., Geoffroy, O., Moene, A. F., Pino, D., de Roode, S. R., and Vil Heus, T., van Heerwaarden, C. C., Jonker, H. J. J., Pier Siebesma, A., Axelsen, S., van den Dries, K., Geoffroy, O., Moene, A. F., Pino, D., de Roode, S. R., and Vila-Guerau de Arellano, J.: Formulation of the Dutch Atmospheric Large-Eddy Simulation (DALES) and overview of its applications, Geosci. Model Dev., 3, 415–444, doi:10.5194/gmd-3-415-2010, 2010. 31531, 31532
Kaimal, J. C., Wyngaard, J. C., Haugen, D. A., Coté, O. R., Izumi, Y., Caughey, S. J., and Readings, C. J.: Turbulence structure in the convective boundary layer, J. Atmos. Sci., 33, 2152–2169, 1976. 31529
Lapworth, A.: The morning transition of the nocturnal boundary layer, Bound.-Lay. Meteorol., 119, 501–526, 2006. 31530

ACPD
13, 31527–31562, 2013

LeMone, M. A., Zhou, M., Moeng, C.-H., Lenschow, D. H., Miller, L. J., and Grossman, R. L.: An observational study of wind profiles in the baroclinic convective mixed layer, Bound.-Lay. Meteorol., 90, 47–82, 1999. 31534

LeMone, M. A., Grossman, R. L., Mcmillen, R. T., Liou, K.-N., Ou, S. C., Mckeen, S., Angevine, W., Ikeda, K., and Chen, F.: CASES-97: late-morning warming and moistening of the convective boundary layer over the Walnut River watershed, Bound.-Lay. Meteorol., 104, 1–52, 2002. 31530

Lilly, D. K.: Models of cloud-topped mixed layers under a strong inversion, Q. J. Roy. Meteor. Soc., 94, 292–309, 1968. 31536

Lloyd, J. and Taylor, J. A.: On the temperature dependence of soil respiration, Funct. Ecol., 8, 315–323, 1994.

Lothon, M., Couvreux, F., Durand, P., Hartogensis, O., Legain, D., Lohou, F., Pardyjak, E. R., Pino, D., Reuder, J., Vilà-Guerau de Arellano, J., Alexander, D., Augustin, P., Bargain, E., Barrié, J., Bazile, E., Bezombes, Y., Blay-Carreras, E., van de Boer, A., Boichard, J. L., de Coster, O., Cuxart, J., Dabas, A., Darbieu, C., Deboudt, K., Delbarre, H., Derrien, S., Faloona, I., Flamant, P., Fourmentin, M., Garai, A., Gibert, F., Gioli, B., Graf, A., Groebner, J., Guichard, F., Jonassen, A., von Kroonenbeerg, M., Lenschow, D., Martin, S., Martinez, D., Mastrorillo, L., Moene, A., Molinos, F., Moulin, E., Pietersen, H., Piguet, B., Pique, E., Román-Gascón, C., Saïd, F., Sastre, M., Seity, Y., Steeneveld, G. J., Toscano, P., Traullé, O., Tzanos, D., Yagüe, C., Wacker, S., Wildmann, N., and Zaldei, A.: The Boundary Layer Late Afternoon and Sunset Turbulence 2011 field experiment, in: 20th Symposium on Boundary Layers and Turbulence/18th Conference on Air–Sea Interaction, Boston, Massachusetts, USA, 9–13 July 2012, 14 B.1, 2012. 31530, 31531, 31532

Mahrt, L.: Nocturnal boundary-layer regimes, Bound.-Lay. Meteorol., 88, 255–278, 1998. 31529

Moeng, C.-H.: A large-eddy-simulation model for the study of planetary boundary-layer turbulence, J. Atmos. Sci., 41, 2052–2062, 1984. 31529

Moeng, C.-H. and Sullivan, P. P.: A comparison of shear- and buoyancy-driven planetary boundary layer flows, J. Atmos. Sci., 51, 999–1022, 1994. 31529

Moncrieff, J., Monteny, B., Verhoef, A., Friborg, T., Elbers, J., Kabat, P., de Bruin, H., Soegaard, H., and Taupin, J. D.: Spatial and temporal variations in net carbon flux during HAPEX-Sahel, J. Hydrol., 189, 563–588, 1997. 31543

ACPD
13, 31527–31562, 2013

Morris, G. A., Ford, B., Rappenglück, B., Thompson, A. M., Mefferd, A., Ngan, F., and Lefer, B.: An evaluation of the interaction of morning residual layer and afternoon mixed layer ozone in Houston using ozonesonde data, Atmos. Environ., 44, 4024–4034, 2010. 31531

Nadeau, D. F., Pardyjak, E. R., Higgins, C. W., Fernando, H. J. S., and Parlange, M. B.: A simple model for the afternoon and early evening decay of convective turbulence over different land surfaces, Bound.-Lay. Meteorol., 141, 301–324, 2011. 31530, 31535

Nieuwstadt, F. T. M.: The turbulent structure of the stable, nocturnal boundary layer, J. Atmos. Sci., 41, 2202–2216, 1984. 31529

Nieuwstadt, F. T. M. and Brost, R. A.: The decay of convective turbulence, J. Atmos. Sci., 43, 532–546, 1986. 31529

Ouwersloot, H. G., Vilà-Guerau de Arellano, J., Nölscher, A. C., Krol, M. C., Ganzeveld, L. N., Breitenberger, C., Mammarella, I., Williams, J., and Lelieveld, J.: Characterization of a boreal convective boundary layer and its impact on atmospheric chemistry during HUMPPA-COPEC-2010, Atmos. Chem. Phys., 12, 9335–9353, doi:10.5194/acp-12-9335-2012, 2012. 31530

Pino, D., and Vilà-Guerau de Arellano, J.: Effects of shear in the convective boundary layer: analysis of the turbulent kinetic energy budget, Acta Geophys., 56, 167–193, 2008. 31529, 31546

Pino, D., Vilà-Guerau de Arellano, J., and Duynkerke, P. G.: The contribution of shear to the evolution of a convective boundary layer, J. Atmos. Sci., 60, 1913–1926, 2003. 31529, 31534

Pino, D., Vilà-Guerau de Arellano, J., and Kim, S. W.: Representing sheared convective boundary layer by zeroth- and first-order-jump mixed-layer models: large-eddy simulation verification, J. Appl. Meteorol. Climatol., 45, 1224–1243, 2006a. 31538

Pino, D., Jonker, H. J. J., Vilà-Guerau de Arellano, J., and Dosio, A.: Role of shear and the inversion strength during sunset turbulence over land: characteristic length scales, Bound.-Lay. Meteorol., 121, 537–556, 2006b. 31529, 31530

Pino, D., Vil Pino, D., Vila-Guerau de Arellano, J., Peters, W., Schröter, J., van Heerwaarden, C. C., and Krol, M. C.: A conceptual framework to quantify the influence of convective boundary layer development on carbon dioxide mixing ratios, Atmos. Chem. Phys., 12, 2969–2985, doi:10.5194/acp-12-2969-2012, 2012.31545

Seibert, P., Beyrich, F., Gryning, S. E., Joffre, S., Rasmussen, A., and Tercier, P.: Review and intercomparison of operational methods for the determination of the mixing height, Atmos. Environ., 34, 1001–1027, 2000. 31537

ACPD
13, 31527–31562, 2013

Soegaard, H.: Fluxes of carbon dioxide, water vapour and sensible heat in a boreal agricultural area of Sweden – scaled from canopy to landscape level, Agr. Forest Meteorol., 98–99, 463–478, 1999. 31543

Sorbjan, Z.: Effects caused by varying the strength of the capping inversion based on a large eddy simulation model of the shear-free convective boundary layer, J. Atmos. Sci., 53, 2015–2024, 1996. 31529, 31530, 31540

Sorbjan, Z.: Decay of convective turbulence revisited, Bound.-Lay. Meteorol., 82, 503–517, 1997. 31530

Sorbjan, Z.: A numerical study of daily transitions in the convective boundary layer, Bound.-Lay. Meteorol., 123, 365–383, 2007. 31529

Stensrud, D. J.: Elevated residual layers and their influence on surface boundary-layer evolution, J. Atmos. Sci., 50, 2284–2293, 1993. 31530

Stull, R. B. (Ed.): An Introduction to Boundary Layer Meteorology, Kluwer Academic Publisher, Dordrecht, the Netherlands, 1988. 31529, 31540

Sullivan, P. P., Moeng, C.-H., Stevens, B., Lenschow, D. H., and Mayor, S. D.: Structure of the entrainment zone capping the convective atmospheric boundary layer, J. Atmos. Sci., 55, 3042–3064, 1998. 31529, 31538, 31540

Tennekes, H.: A model for the dynamics of the inversion above a convective boundary layer, J. Atmos. Sci., 30, 558–567, 1973. 31529, 31536

Tennekes, H. and Driedonks, A. G. M.: Basic entrainment equations for the atmospheric boundary layer, Bound.-Lay. Meteorol., 20, 515–531, 1981. 31529, 31531, 31533, 31536

Vilà-Guerau de Arellano, J., van den Dries, K., and Pino, D.: On inferring isoprene emission surface flux from atmospheric boundary layer concentration measurements, Atmos. Chem. Phys., 9, 3629–3640, doi:10.5194/acp-9-3629-2009, 2009. 31529

Wehner, B., Siebert, H., Ansmann, A., Ditas, F., Seifert, P., Stratmann, F., Wiedensohler, A., Apituley, A., Shaw, R. A., Manninen, H. E., and Kulmala, M.: Observations of turbulence-induced new particle formation in the residual layer, Atmos. Chem. Phys., 10, 4319–4330, doi:10.5194/acp-10-4319-2010, 2010. 31529

Yi, C., Davis, K. J., Berger, B. W., and Bakwin, P. S.: Long-term observations of the dynamics of the continental planetary boundary layer, J. Atmos. Sci., 58, 1288–1299, 2001. 31529, 31534, 31544

ACPD
13, 31527–31562, 2013

Table 1. Based on the observations taken at the BLLAST campaign on 1 July 2011, initial and prescribed values used for DALES (RL and nRL numerical experiments) and MLM of the boundary-layer depth, mixed-layer and residual layer values of the scalars ($\theta_{1,0}$, $\theta_{RL,0}$ and $q_{1,0}$, $q_{RL,0}$) and their corresponding jump at the inversion ($\Delta\theta_{1,0}$, $\Delta\theta_{RL,0}$, $\Delta q_{1,0}$ and $\Delta q_{RL,0}$). γ_i is the FA lapse rate of each variable i. Surface fluxes ($\overline{w'\theta'}|_s$ and $\overline{w'q'}|_s$) are prescribed as $0.1668\sin(\pi(t-5)/12.5)$ and $0.1032\sin(\pi(t-5.5)/13.5)$ respectively. Time t goes from 0 (07:30 UTC) to 45 000 s (20:00 UTC).

	RL	nRL	MLM (11:00 UTC)
$\theta_{1,0}$ (K)	293	293	295.5
$\Delta\theta_{1,0}$ (K)	2	5	8
$z_{1,0}$ (m)	210	210	1300
$\theta_{RL,0}$ (K)	295	–	–
$\Delta\theta_{RL,0}$ (K)	9	–	–
$z_{RL,0}$ (m)	1422	–	–
γ_θ (K m^{-1})	0.005	0.005	0.005
$q_{1,0}$ (g kg^{-1})	7.16	7.16	8
$\Delta q_{1,0}$ (g kg^{-1})	−1.66	−5.66	−5
$q_{RL,0}$ (g kg^{-1})	5.50	–	–
$\Delta q_{RL,0}$ (g kg^{-1})	−4.41	–	–
γ_q (g (kg m)$^{-1}$)	−0.00035	−0.00035	−0.00035

ACPD
13, 31527–31562, 2013

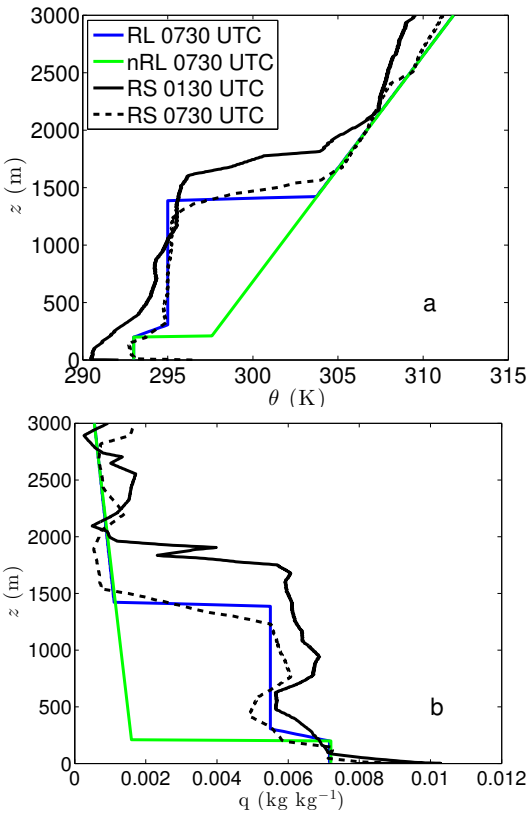

Fig. 1. Vertical profile of **(a)** potential temperature and **(b)** specific humidity observed by the radio soundings launched at 01:30 (solid black) and at 07:30 UTC (dashed black) on 1 July 2011. Additionally, the vertical profiles based in the observations for initializing the DALES RL numerical experiments (solid blue) and nRL numerical experiments (solid green) are shown. Table 1 shows the values which characterize initial profile of θ and q.

ACPD
13, 31527–31562, 2013

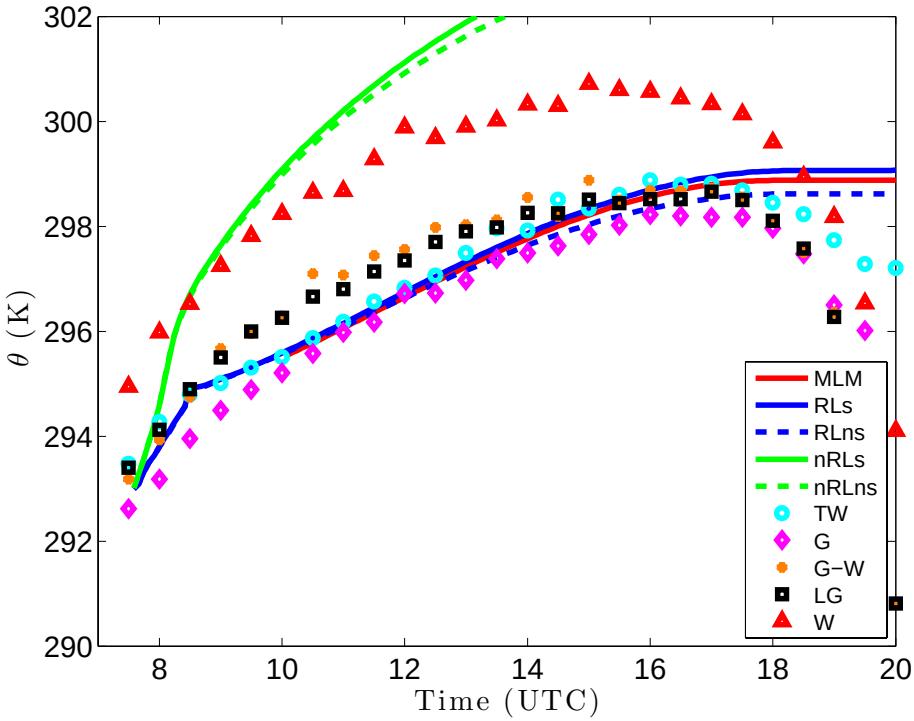

Fig. 2. Temporal evolution of potential temperature on 1 July 2011 observed by different instruments at 2 m (symbols) and obtained (lines) by MLM with subsidence (red) and DALES (RLs, solid blue; RL, dash blue; nRLs, solid green; and nRL, dash green). Observations are from EC instrument at the tower over grass (TW, cyan circles), over short grass (G, magenta diamonds), over the edge between the long grass and the wheat (G–W, orange dots), over long grass (LG, black squares) and over wheat (W, red triangles).

ACPD
13, 31527–31562, 2013

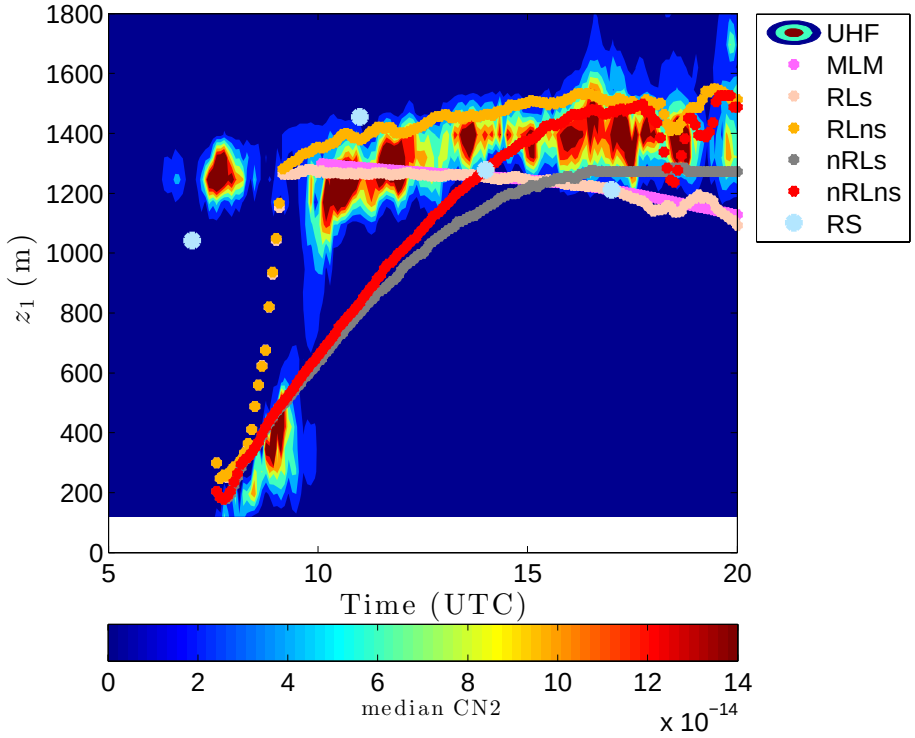

Fig. 3. Time evolution during 1 July 2011 of the refractive structure coefficient measured by UHF wind profiler (color contour), and boundary layer depth estimated from radio soundings (light blue dots), and obtained by MLM (magenta line), and DALES numerical experiments (RLs, pink; RL, orange; nRLs, grey; and nRL, red lines).

ACPD
13, 31527–31562, 2013

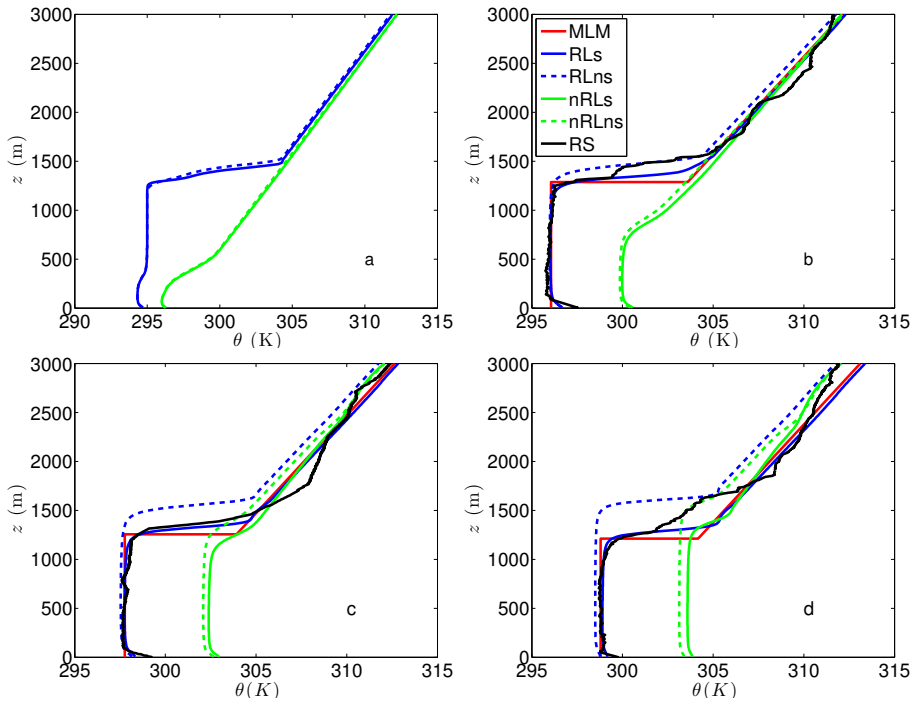

Fig. 4. Vertical profile of the 30 min averaged potential temperature at **(a)** 08:30, **(b)** 11:00, **(c)** 14:00 and **(d)** 17:00 UTC on 1 July 2011 observed by the radio soundings (solid black) and obtained by MLM (solid red) and DALES numerical experiments (RLs, solid blue; RL, dash blue; nRLs, solid green; and nRL, dash green line).

ACPD
13, 31527–31562, 2013

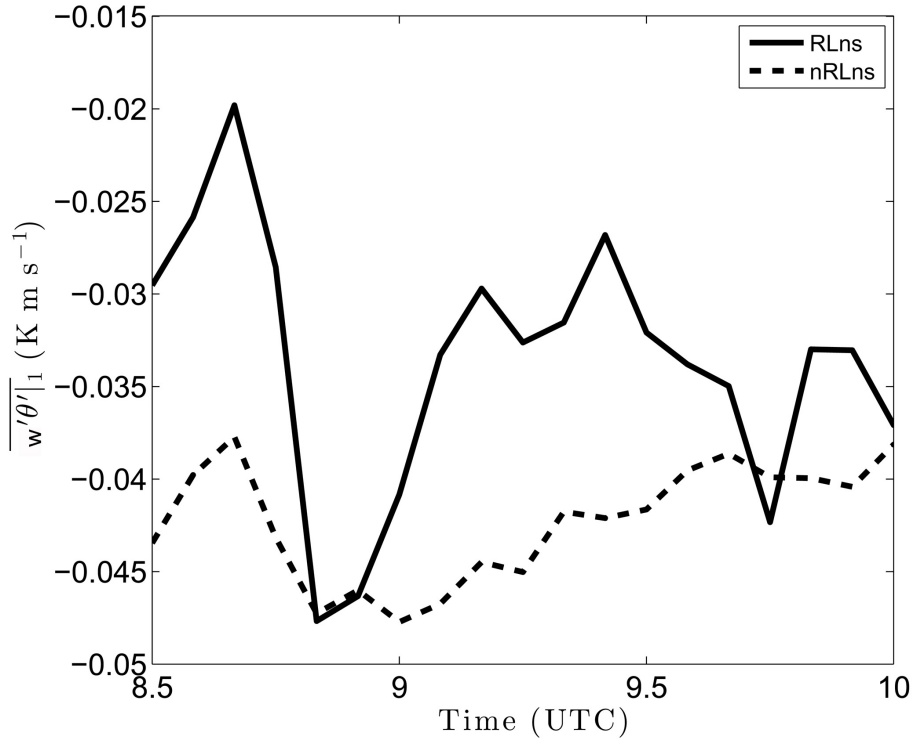

Fig. 5. Temporal evolution during the morning of the entrainment heat flux for the RLns (solid line) an nRLns (dashed line) DALES numerical experiments.

ACPD
13, 31527–31562, 2013

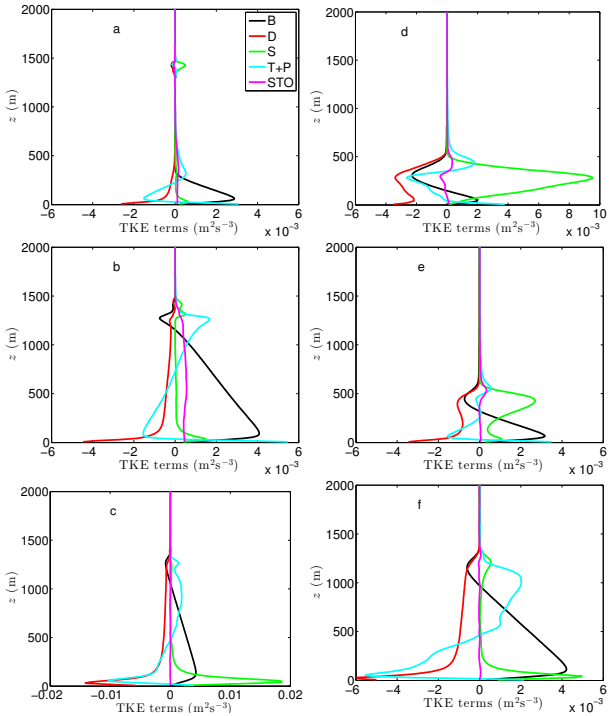

Fig. 6. Vertical profiles of the 30 min averaged TKE-terms for the (left) RLns and (right) nRLNs numerical experiments at (top) 08:30, (middle) 09:00 and (bottom) 14:00 UTC. Buoyancy production (black line), dissipation (red line), shear production (green line), turbulent transport and pressure (cyan line) and storage (magenta line) are shown.

ACPD
13, 31527–31562, 2013

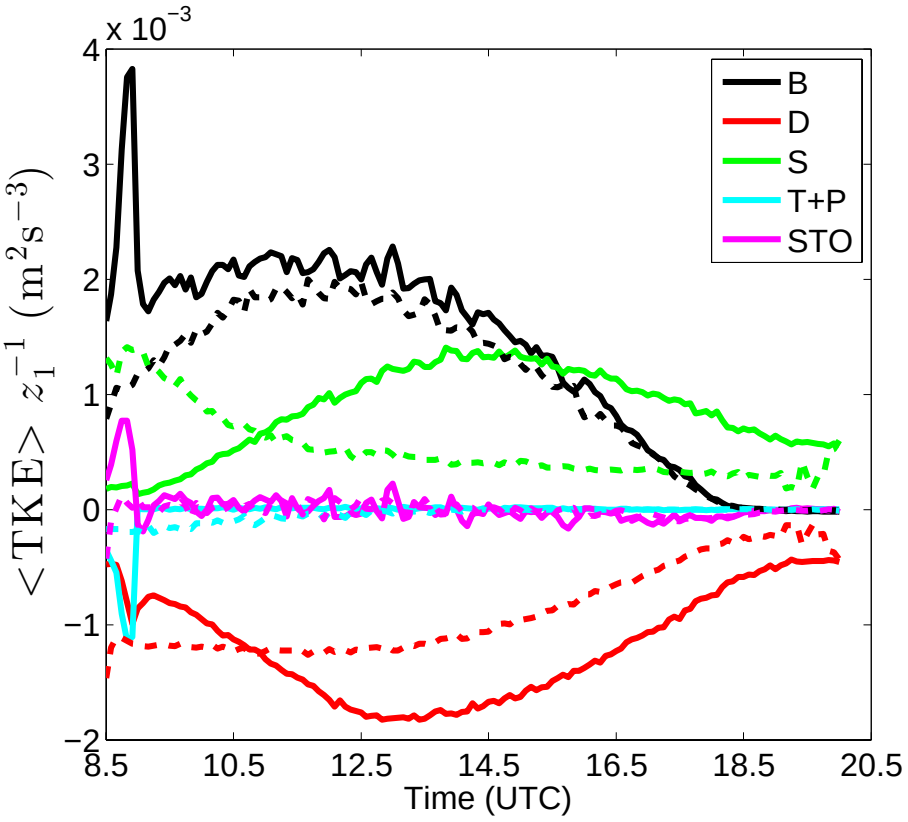

Fig. 7. Temporal evolution of each vertically averaged (from 0 to z_1) TKE-term normalized by z_1 for (solid) RLns and (dashed) nRLns numerical experiments.

ACPD
13, 31527–31562, 2013

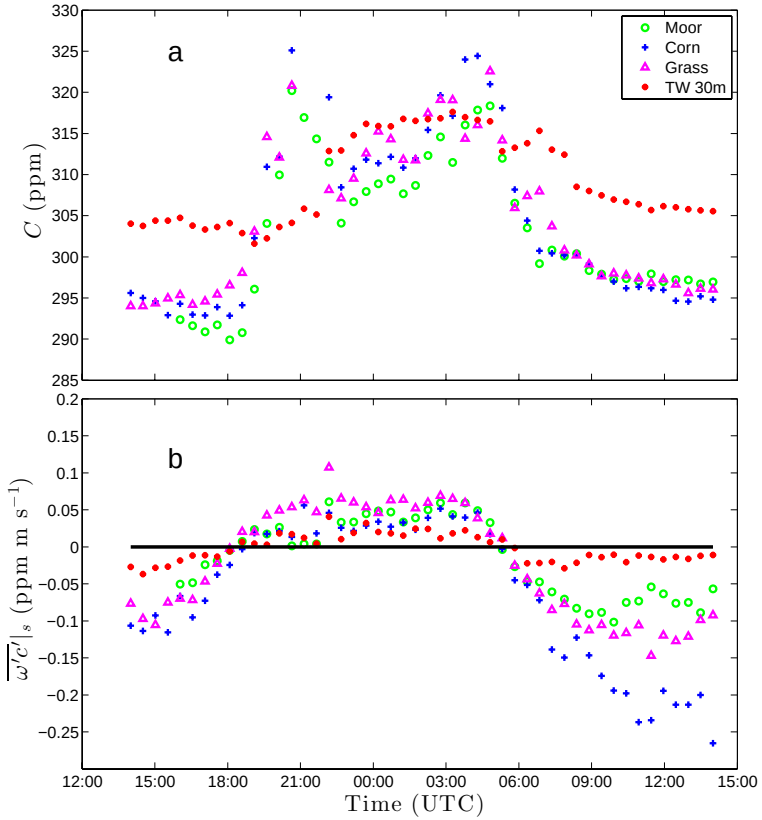

Fig. 8. Temporal evolution from 30 June 2011 at 14:00 UTC to 1 July 2011 at 14:00 UTC of the observed **(a)** CO_2 mixing ratio and **(b)** CO_2 surface flux measured at 2 m over moor (green circles), over corn (blue crosses), over long grass (magenta triangles) and at 30 m over grass (red asterisks).

ACPD
13, 31527–31562, 2013